

Supporting Information

Impact of the F⁻ for O²⁻ substitution in Na₃V₂(PO₄)₂F_{3-y}O_y on their transport properties and electrochemical performance

Runhe Fang ^{a,d}, Jacob Olchowka ^{b,d,e,*}, Chloé Pablos ^{b,c,d}, Rafael Bianchini
Nuernberg ^b, Laurence Croguennec ^{b,d,e}, Sophie Cassaignon^{a,d,*}

^a Sorbonne Université, CNRS, Laboratoire Chimie de la Matière Condensée de Paris,
LCMCP, UMR 7574, 4 Place Jussieu, 75005 Paris, France

^b Univ. Bordeaux, CNRS, Bordeaux INP, ICMCB, UMR 5026, F-33600 Pessac, France

^c Laboratoire de Réactivité et de Chimie des Solides, Université de Picardie Jules Verne,
CNRS-UMR 7314, F-80039 Amiens Cedex 1, France

^d RS2E, Réseau Français sur le Stockage Electrochimique de l'Energie, CNRS 3459,
80039 Amiens Cedex 1, France.

^e ALISTORE-ERI European Research Institute, CNRS 3104, 80039 Amiens Cedex 1, France

* Corresponding authors:

S. Cassaignon (sophie.cassaignon@sorbonne-universite.fr)

J. Olchowka (jacob.olchowka@icmcb.cnrs.fr)

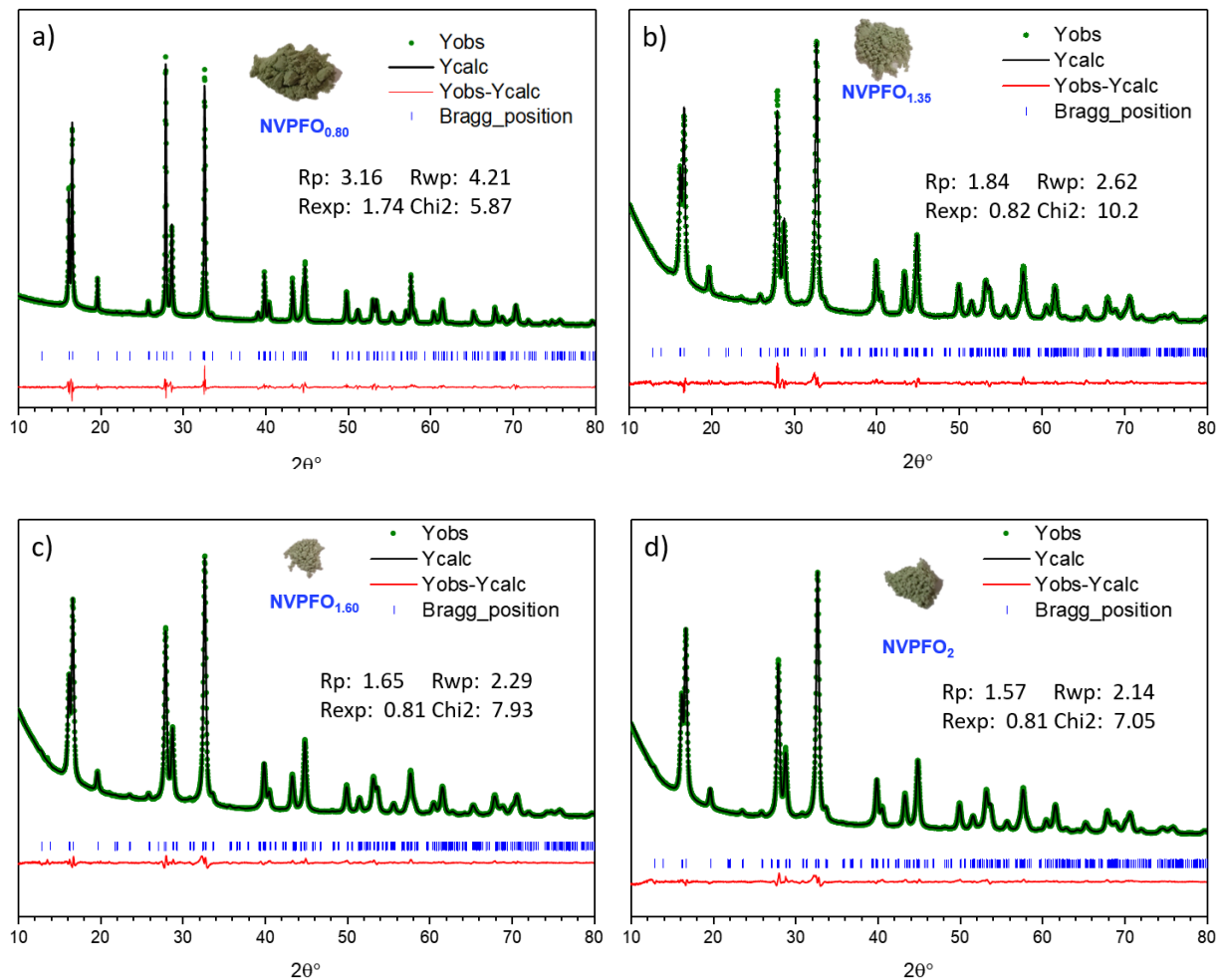


Figure S1. Rietveld refinement of the XRD data for the different compounds NVPFO_{0.80}, NVPFO_{1.35}, NVPFO_{1.60} and NVPFO₂.

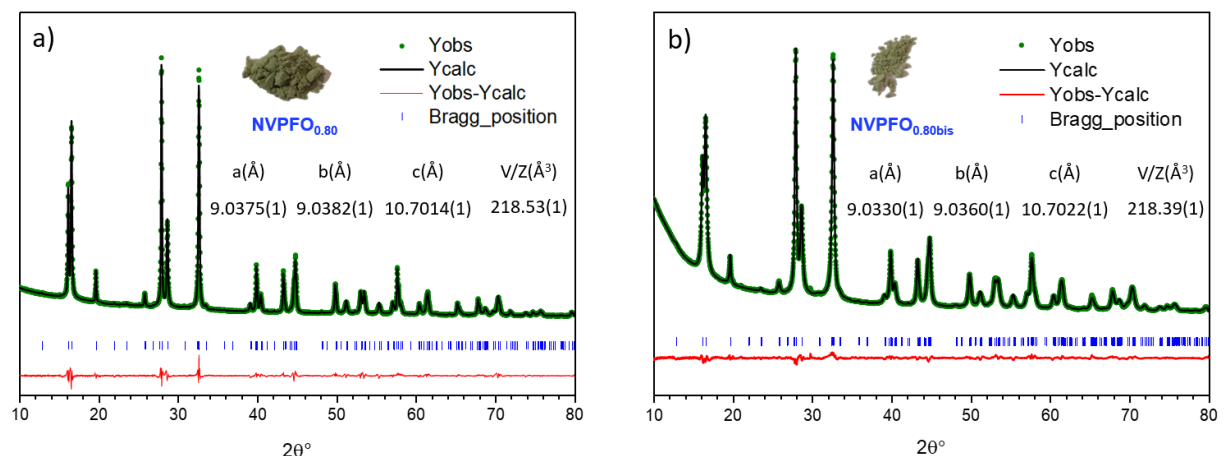


Figure S2. The cell parameter comparison of the NVPFO_{0.80} and NVPFO_{0.80bis}

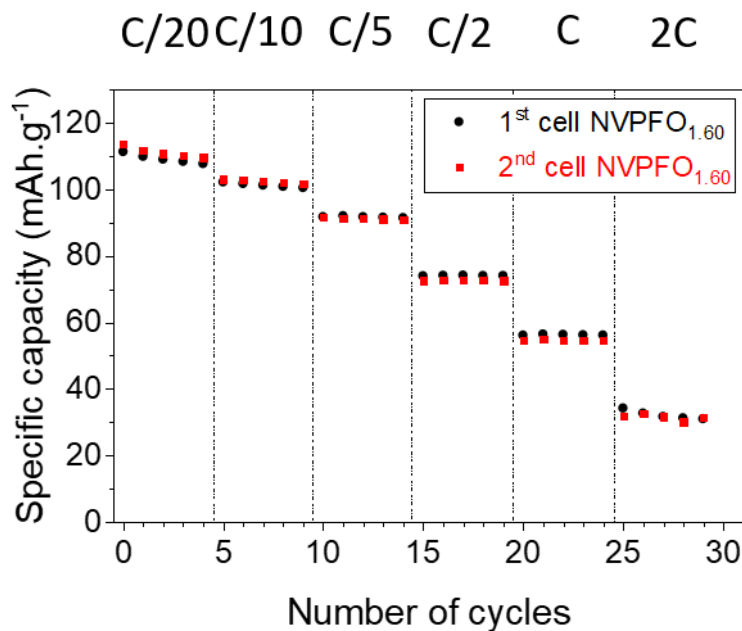


Figure S3. Illustration of the reproducibility of the electrochemical performance obtained for NVPFO_{1.6}.

This shows an example of the reproducibility of the electrochemical tests that were performed for NVPFO_{1.6}. The reproducibility tests validate that the different performance in the study are induced by the different chemical composition and not influenced by the experimental cell assembly.

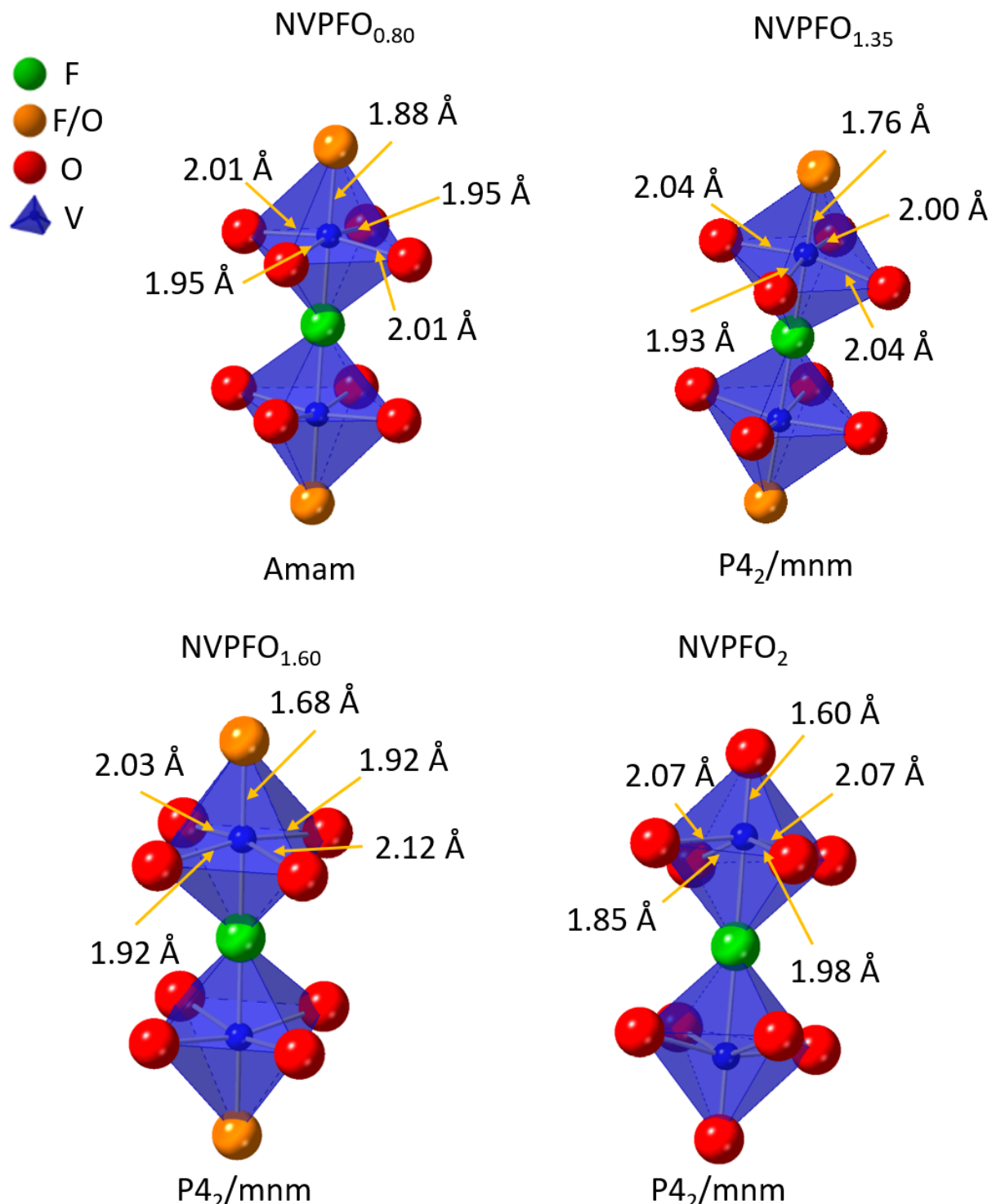


Figure S4. Illustration of bond distance changes from the composition $\text{NVPFO}_{0.80}$ to the composition NVPFO_2 .

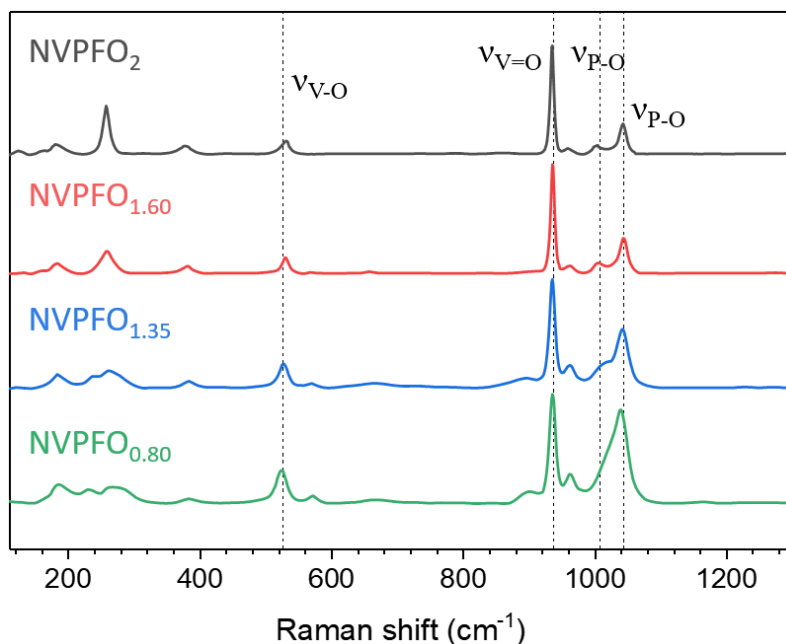


Figure S5. All Raman spectra from 100 cm^{-1} to 1300 cm^{-1} . The spectra were corrected to remove the background. The absence of signal after 1150 cm^{-1} confirmed the absence of carbon in the compounds (absence of D-band, see Figure S6)¹.

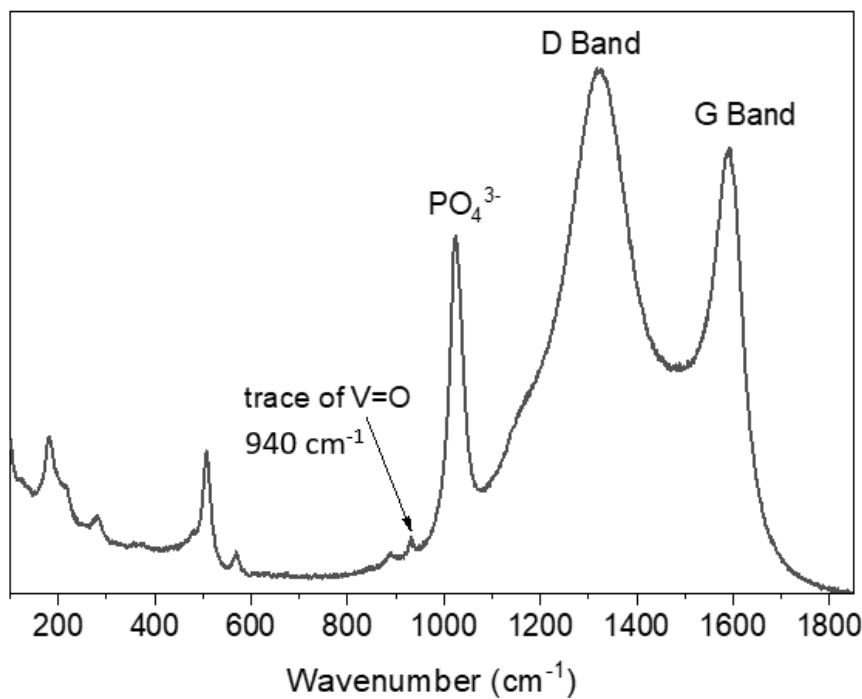


Figure S6. Raman spectrum of carbon-coated $\text{Na}_3\text{V}_2(\text{PO}_4)_2\text{F}_3$ ($y=0$). The electrode material was synthesized through the method proposed by Hall et al.² This spectrum confirms the absence of carbon in the series studied in this work (absence of signal around $1150\text{-}1300\text{ cm}^{-1}$ as shown in Figure S5) and endorses the attribution of the signal at 940 cm^{-1} to vanadyl bond vibration since this signal nearly disappears for $\text{Na}_3\text{V}^{3+}_2(\text{PO}_4)_2\text{F}_3$. Indeed, as reported previously, a small amount of vanadyl type defects is always identified, which explains the detection of the signal at 940 cm^{-1} .³

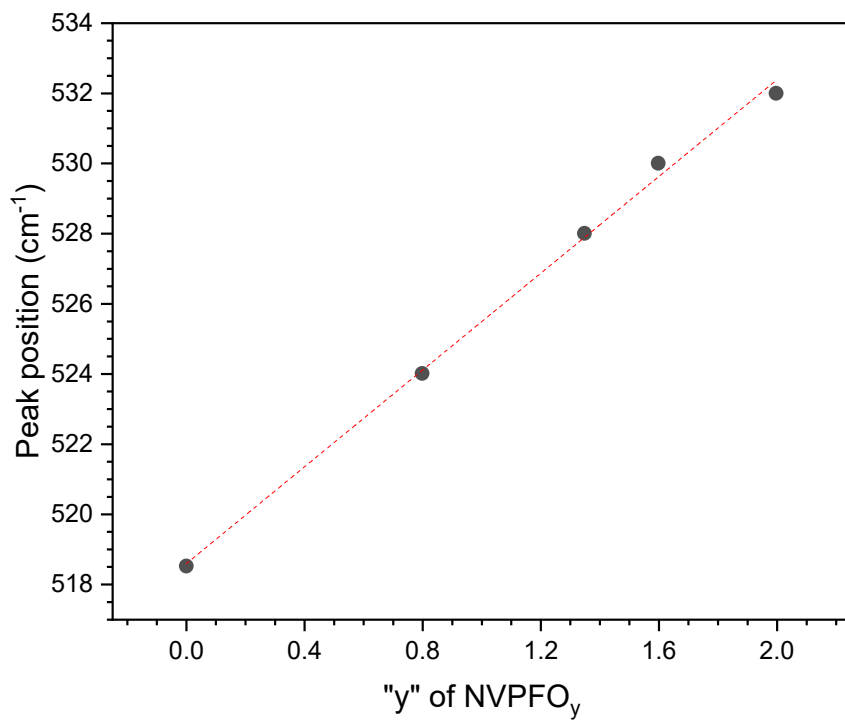


Figure S7. "y" of NVPFO_y variation versus the shift of the V-O peak position. The linear fitting in red clearly demonstrates a linear shift of the peak according to the chemical formulae. The position of V-O band for NVPF3 ($y=0$) is measured from the spectrum reported in figure S6.

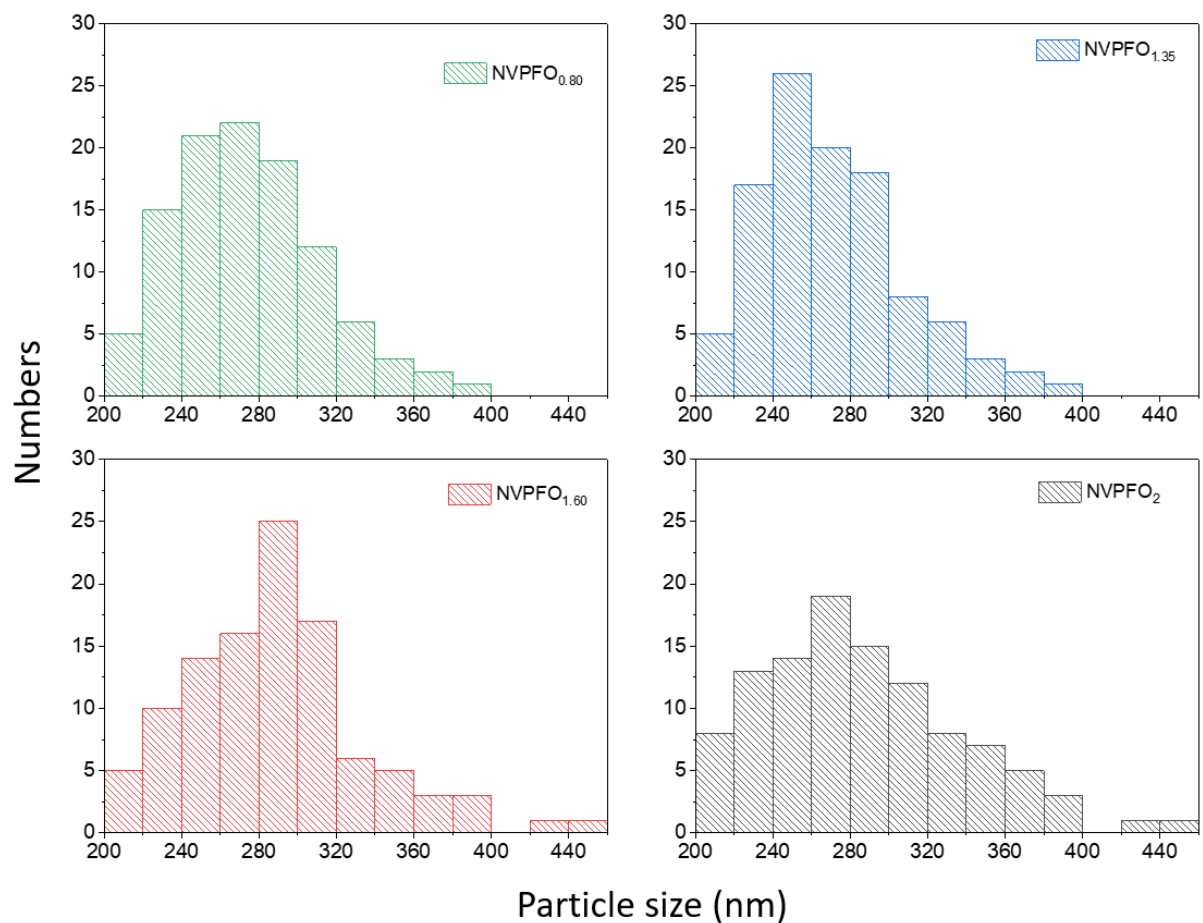


Figure S8. Statistics of particle size distribution for all the materials. For each material 106 particles were measured.

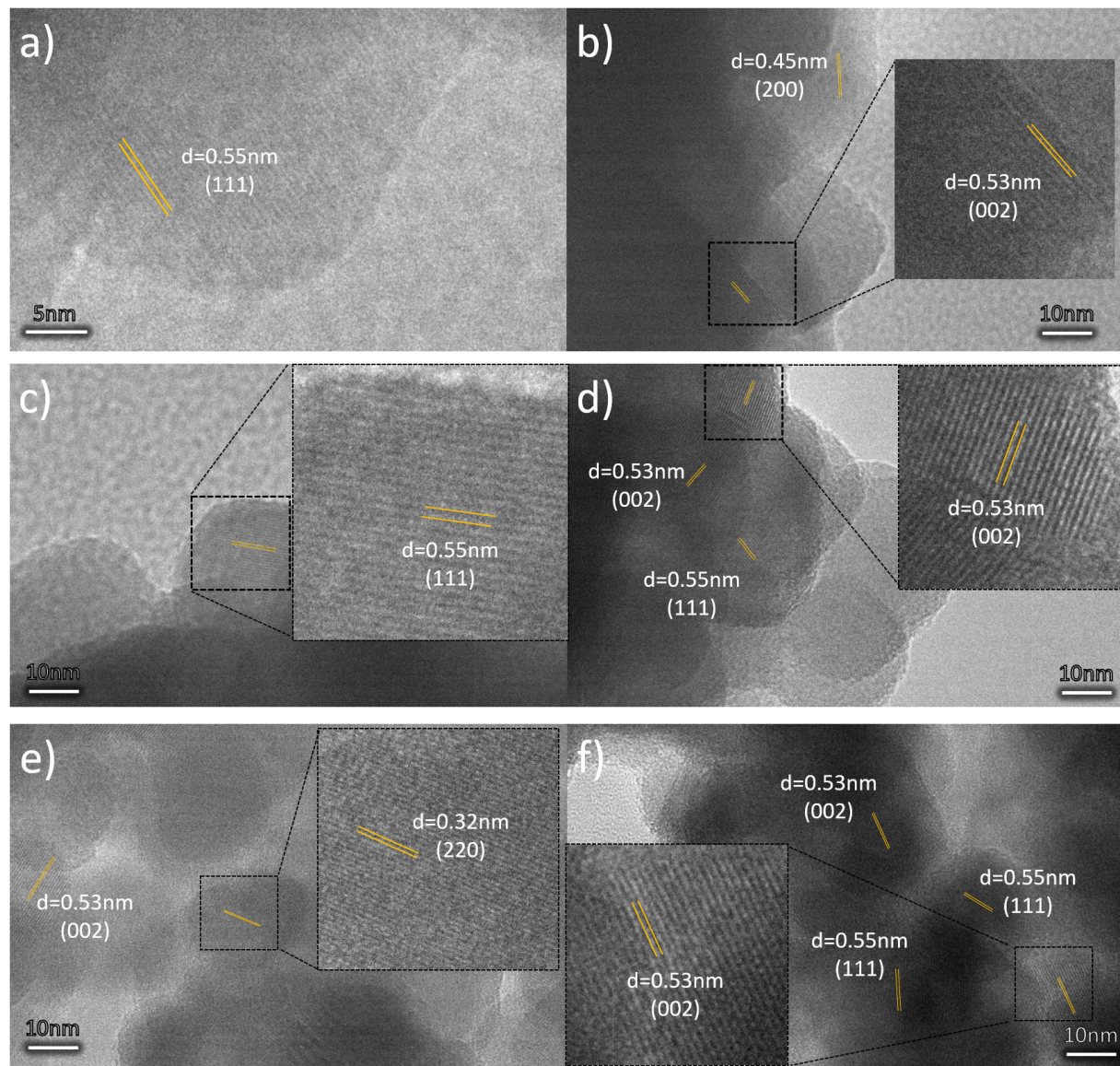


Figure S9. HRTEM images of a-b) NVPFO_{0.80}, c-d) NVPFO_{1.60} and e-f) NVPFO₂.

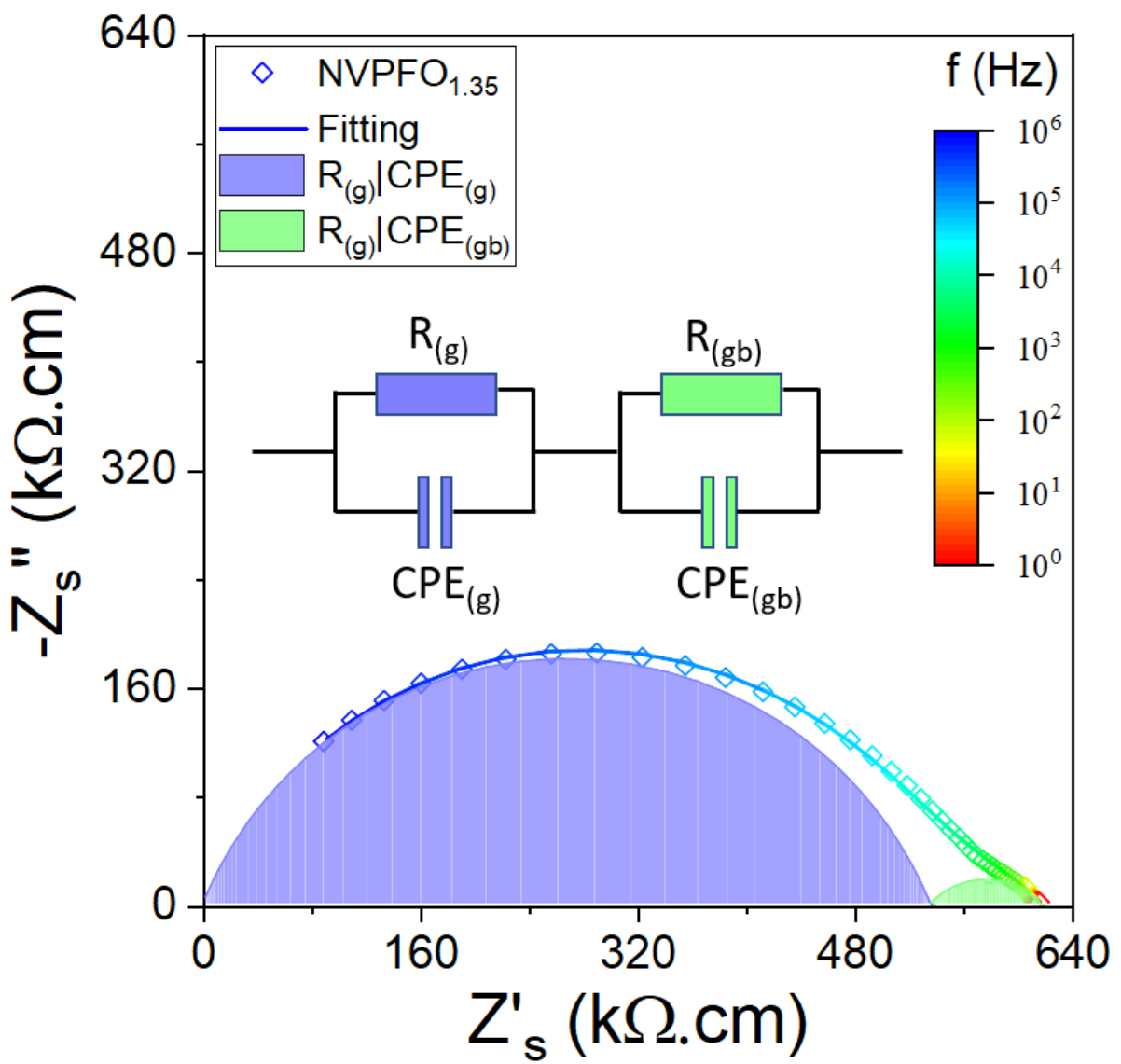


Figure S10. Deconvolution of grain and grain boundary contributions of complex impedance data recorded at 200 °C for NVPFO_{1.35} sample. The complex impedance data shown here have already been normalized regarding the shape factor of the sample. The shown equivalent circuit is used for impedance data fitting. Acronyms R and CPE represent resistive and constant phase elements whereas g and gb stand for grain and grain boundary contributions, respectively. The obtained effective specific capacitances or the relative permittivities are typical from grain (1.4 pF.cm⁻¹ or 15) and grain boundary (470 pF.cm⁻¹ or 5329⁴) contributions.

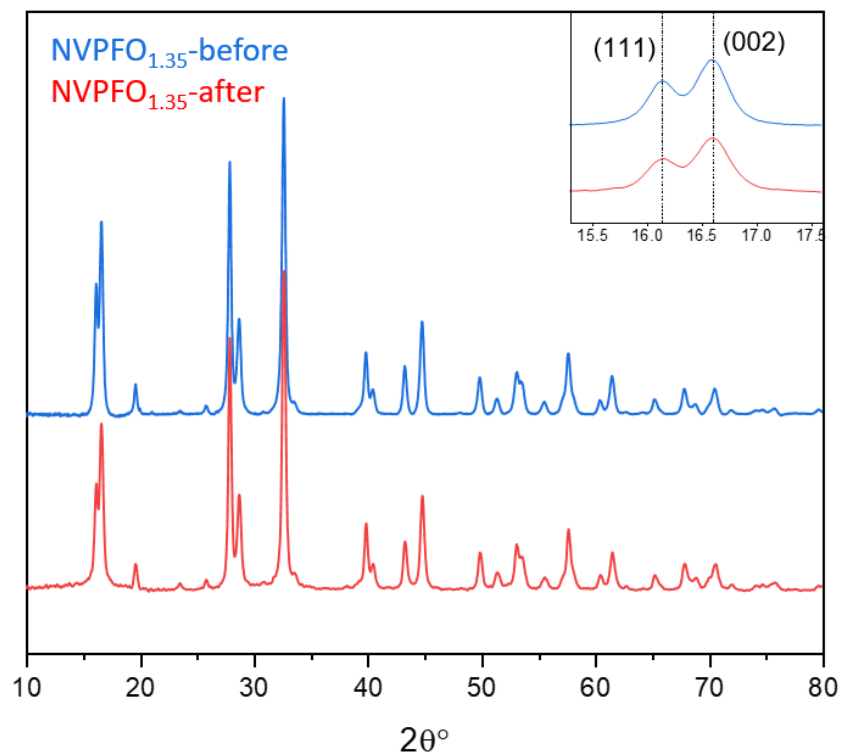


Figure S11. Comparison of the XRD patterns collected for $\text{NVPFO}_{1.35}$, before and after the impedance measurement, with inset of enlarged (111) and (002) peaks.

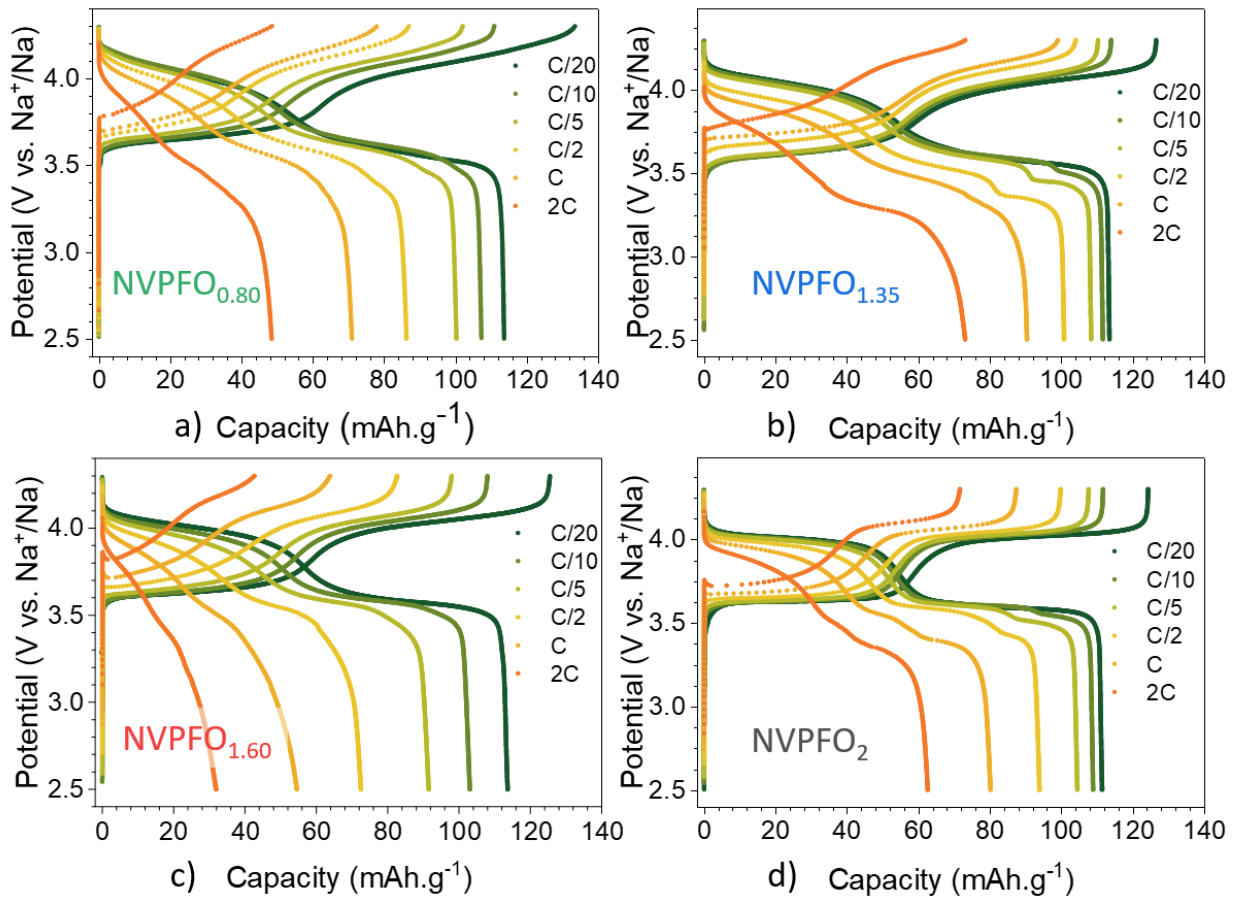


Figure S12. Charge and discharge curves of NVPFO_y materials at different cycling rates, from C/20 to 2C.

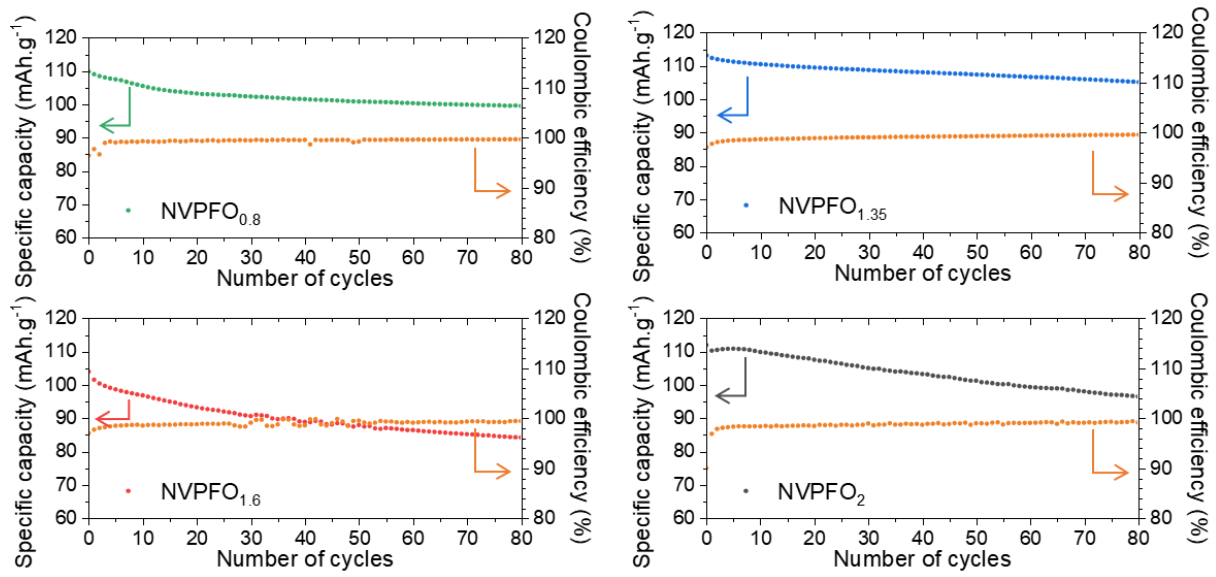


Figure S13. Long range cycling performance (specific capacity and Coulombic efficiency) at C/10 for NVPFO_y.

Bibliography:

- (1) Cai, Y.; Cao, X.; Luo, Z.; Fang, G.; Liu, F.; Zhou, J.; Pan, A.; Liang, S. Caging Na₃V₂(PO₄)₂F₃ Microcubes in Cross-Linked Graphene Enabling Ultrafast Sodium Storage and Long-Term Cycling. *Adv. Sci.* **2018**, *5* (9). <https://doi.org/10.1002/advs.201800680>.
- (2) Hall, N.; Boulineau, S.; Croguennec, L.; Launois, S.; Masquelier, C.; Simonin, L. Method For Preparing a Na₃V₂(PO₄)₂F₃ Particulate Material. *United States Pat.* **2018**.
- (3) Nguyen, L. H. B.; Broux, T.; Camacho, P. S.; Denux, D.; Bourgeois, L.; Belin, S.; Iadecola, A.; Fauth, F.; Carlier, D.; Olchowka, J.; Masquelier, C.; Croguennec, L. Stability in Water and Electrochemical Properties of the Na₃V₂(PO₄)₂F₃ – Na₃(VO)₂(PO₄)₂F Solid Solution. *Energy Storage Mater.* **2019**, *20* (April), 324–334. <https://doi.org/10.1016/j.ensm.2019.04.010>.
- (4) Irvine, J. T. S.; Sinclair, D. C.; West, A. R. Electroceramics: Characterization by Impedance Spectroscopy. *Adv. Mater.* **1990**, *2* (3), 132–138. <https://doi.org/10.1002/ADMA.19900020304>.